nature communications

Article

https://doi.org/10.1038/s41467-023-42723-3

A low-nuclear Ag_4 nanocluster as a customized catalyst for the cyclization of propargylamine with CO_2

Received: 11 April 2023

Accepted: 19 October 2023

Published online: 01 November 2023

Check for updates

Lin Li[1,2,3,5], Ying Lv[1,2,3,5], Hongting Sheng[1,2,3] ✉, Yonglei Du[1,2,3], Haifeng Li[1,2,3], Yapei Yun[2,3], Ziyi Zhang[1,2,3], Haizhu Yu[1,2,3] ✉ & Manzhou Zhu[1,2,3,4] ✉

The preparation of 2-Oxazolidinones using CO_2 offers opportunities for green chemistry, but multi-site activation is difficult for most catalysts. Here, A low-nuclear Ag_4 catalytic system is successfully customized, which solves the simultaneous activation of acetylene (-C≡C) and amino (-NH-) and realizes the cyclization of propargylamine with CO_2 under mild conditions. As expected, the Turnover Number (TON) and Turnover Frequency (TOF) values of the Ag_4 nanocluster (NC) are higher than most of reported catalysts. The Ag_4* NC intermediates are isolated and confirmed their structures by Electrospray ionization (ESI) and ^{1}H Nuclear Magnetic Resonance (^{1}H NMR). Additionally, the key role of multiple Ag atoms revealed the feasibility and importance of low-nuclear catalysts at the atomic level, confirming the reaction pathways that are inaccessible to the Ag single-atom catalyst and Ag_2 NC. Importantly, the nanocomposite achieves multiple recoveries and gram scale product acquisition. These results provide guidance for the design of more efficient and targeted catalytic materials.

The conversion of CO_2 into high-value-added chemicals[1–7], such as starch[8], carboxylic acid[9,10], propylene carbonate[11,12], and 2-oxazolidinone[13], is considered a promising approach to achieve carbon neutrality and has become a hot topic in the field of catalysis. In particular, 2-oxazolidone compounds have important application potential in organic intermediates, antibacterial drugs and chiral auxiliaries[14,15]. Ideally, the greenest preparation of 2-oxazolone compounds is the cyclization of propargylamine with CO_2. However, due to the unique structure of propargylamine, which contains both acetylene (-C≡C) and amino (-NH-) functional groups, it is difficult for most current catalysts to achieve this transformation[16–19]. Therefore, there is an urgent need to customize a catalyst with multiple active sites for the cyclization of propargylamine with CO_2.

Single-atom catalysts (SACs) have been widely used for CO_2 conversion due to their high molar utilization, clear active site, and unique electronic structure[20–23]. However, the presence of only a single metal site inherently limits SACs performance[24–28]. In contrast, low-nuclear nanoclusters (NCs) not only show the same characteristics as SACs but also benefit from synergistic effects between adjacent metals[29–36]. However, low-nuclear-weight NCs are more prone to unpredictable structural transformations under harsh environments[37,38], making it difficult to identify the true active component. Scott et al. reported that alkyne-protected Cu_{20} NC do not require harsh pretreatment during catalysis[39], Wang et al. reported that an alkyne-protected Au_{38} NC exhibited superior performance compared to that of a sulfate-protected Au_{38} NC[40]. Zheng et al. found that the activity of intact $Au_{34}Ag_{28}(PhC{\equiv}C)_3$ is significantly better than that of partially or completely removed ligands[41]. Alkyne ligands, as metal-organic ligands, are considered to play an important role in improving the catalytic performance[42–44].

[1]Department of Chemistry and Centre for Atomic Engineering of Advanced Materials, Anhui University, Hefei 230601, China. [2]Key Laboratory of Structure and Functional Regulation of Hybrid Materials of Ministry of Education, Hefei 230601, China. [3]Key Laboratory of Functional Inorganic Material Chemistry of Anhui Province, Anhui University, Hefei 230601, China. [4]Anhui Tongyuan Environment Energy Saving Co., Ltd., Hefei 230041, China. [5]These authors contributed equally: Lin Li, Ying Lv. ✉e-mail: shenght@ahu.edu.cn; yuhaizhu@ahu.edu.cn; zmz@ahu.edu.cn

Therefore, we designed a low-nuclear Ag_4 NC protected by alkynes for the cyclization of propargylamine with CO_2. As expected, the customized Ag_4 NC achieved the highest TON value of 5746.2, significantly higher than that of reported catalysts and the corresponding Ag_2 NC, Ag_6 NC and Ag_9 NC. Moreover, three Ag_4 *NC intermediates were captured and confirmed their structures by ESI and ^{1}H NMR. The key role of four Ag atoms revealed the feasibility and importance of low-nuclear catalysts at the atomic level. More importantly, the obtained Ag_4/TNT nanocomposite afforded the product at the gram scale.

Result and discussion

A low-nuclear alkyne-protected Ag_4 NC and the corresponding Ag_6 NC and Ag_9 NC were synthesized according to the literatures[45–47]. All these Ag NCs were characterized by mass spectrometry, UV–vis absorption spectroscopy, and single-crystal diffraction analysis (Fig. 1a and Supplementary Figs. S1–S3), confirming the atomic monodispersity and the exact formula assigned to Ag_4 NC, Ag_6 NCand Ag_9 NC, respectively. N-Benzylprop-2-yn-1-amine (**1a**, $HC{\equiv}CCH_2NHBn$) was selected as the preferred substrate for the cyclization of propargylamine to explore the catalytic performance of the customized Ag_4 NC. As expected, the Ag_4 NC protected by the acetylene ligand showed the best performance. To exclude the influence of the number of metal atoms, we designed and synthesized Ag_2 NC through a controlled experiment and compared their activity (Fig. 1a and Supplementary Fig. 4). Interestingly, among the Ag_n (n = 2,4,6,9) NC series, Ag_4 NC had the highest catalytic activity with TON and TOF values up to 5746.2 and 2873.1 h^{-1}, respectively, which were higher than those of reported catalysts (Fig. 1b and Supplementary Table 3). Then, we investigated the catalytic activity of $AgNO_3$, $AgBF_4$ and $[Ag(C{\equiv}C^tBu)]_n$, and the results show that the activity of these catalysts is low. Furthermore, the Ag_4 NC with a Dppf (1,1′-Bis(diphenylphosphino)ferrocene) ligand was inactive for this reaction (Fig. 1b and Supplementary Table 1). The changes in the kinetics of the cyclization of N-benzylprop-2-yn-1-amine with CO_2 catalyzed by low-nuclear Ag_4 NC were monitored by in situ ^{1}H NMR (Supplementary Fig. 5a). Under the ideal conditions, we further explored the generality of the reaction for various propargylamine substrates. As shown in Fig. 1c and Supplementary Table 2, Ag_4 NC afforded the target products in high yields within 2 h for all propargylamine substrates (**3a**-**4a**) with alkyl terminations. Moreover, Ag_4 NC also reacted satisfactorily and afforded the corresponding products for substrates (**5a**-**7a**) with either electron-withdrawing or electron-donating groups. Most studies have reported that the low nucleophilicity of substrates such as N-phenylpropyl-2-yn-1-amine (**2a**) prevents the nucleophilic attack of carbon dioxide due to the benzene ring, resulting in a carbamate intermediate that is difficult to convert smoothly or requires high temperature conditions[16,48]. Much to our surprise and delight, the customized Ag_4 NC achieved highly active conversion of the N-phenylpropyl-2-yn-1-amine substrate at room temperature with yields up to 87%.

On this basis, we conducted relevant control experiments to gain more insight into the fundamental source of the catalytic activity of Ag_4 NC. The characteristic UV peak of Ag_4 NC showed a slight blueshift (8 nm) after Ag_4 NC was mixed with substrate 1a (1:2) for 1 h. In contrast, the characteristic peak of Ag_4 NC did not change at all within 2 h (Supplementary Fig. 5a). The adsorption of **1a** on the Ag_4 NC was detected by Fourier Transform Infrared (FT-IR) Spectroscopy. As shown in Supplementary Fig. 5c, the dominant stretching peak of C≡C-H at 3290 cm^{-1} disappeared, and the peak of C≡C at 2106 cm^{-1} shifted to 2120 cm^{-1}. This reveals that the H atom of C≡C-H was removed from

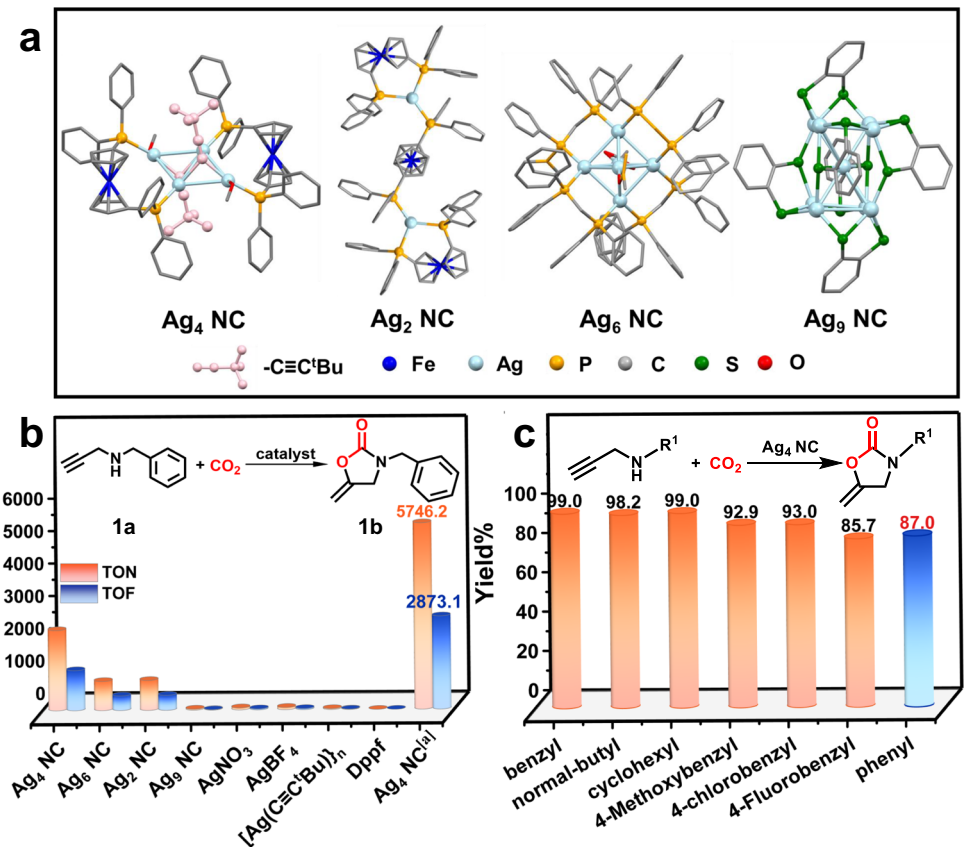

Fig. 1 | Activity comparison and substrate expansion. a Total structure of the Ag_n (n = 2,4,6,9) NCs. **b** TON and TOF value of different catalysts for CO_2 cycloaddition of N-benzylprop-2-yn-1-amine. Reaction conditions: Ag_4 NC (0.04 mol%), propargylamine (0.5 mmol), DBU (0.05 mmol), solvent (1 mL), 25 °C and CO_2 balloon. Yields and selectivity were determined by gas chromatography. [a] propargylamine (1.5 mmol), DBU (0.15 mmol), solvent (1 mL), 25 °C and CO_2 balloon. **c** The cyclization of various propargylamine with CO_2.

https://doi.org/10.1038/s41467-023-42723-3

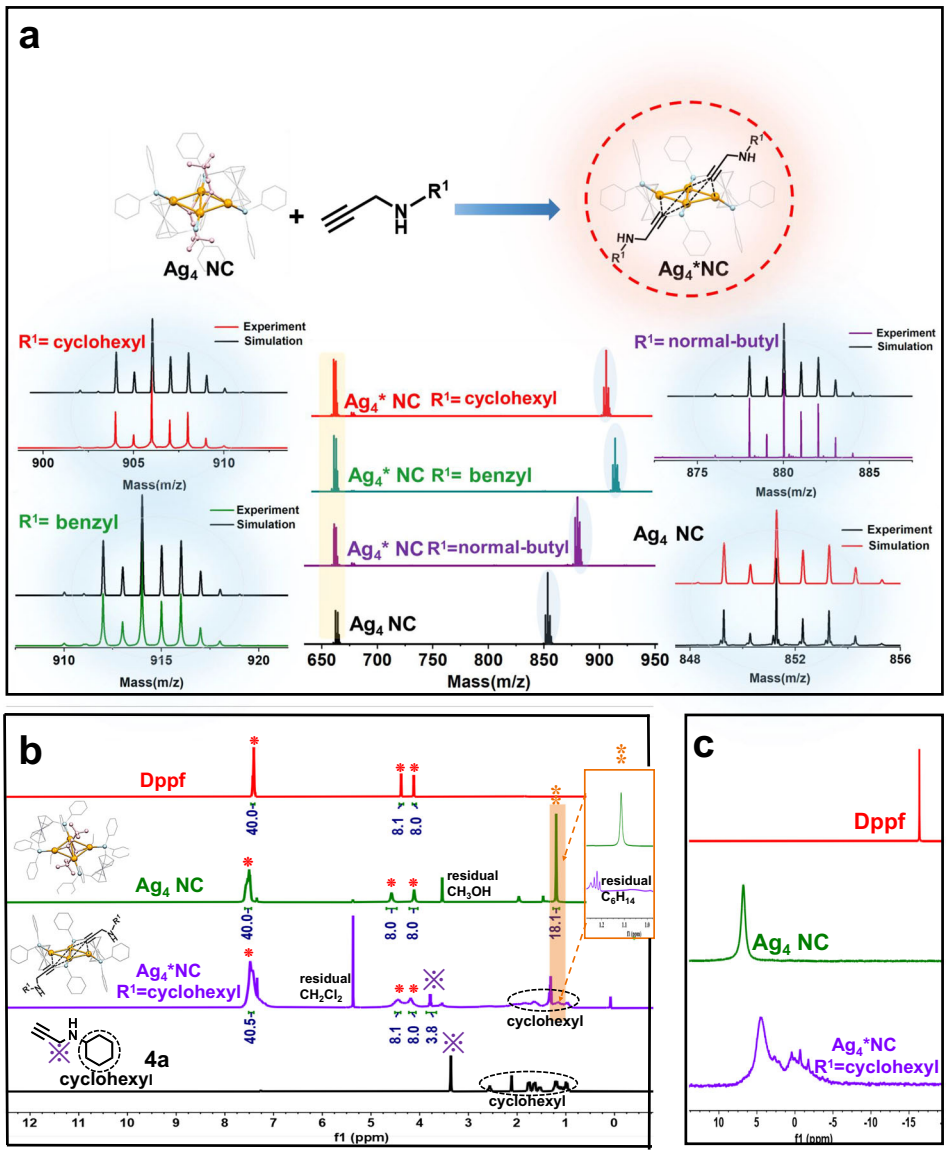

Fig. 2 | Characterization of Ag_4 NC and Ag_4* NC. a ESI-MS spectra of the intermediate Ag_4* NC and simulation of the corresponding mass spectrum. **b** ^{1}H NMR spectra of **4a**, Ag_4* NC R^1 = cyclohexyl, Ag_4 NC, and Dppf. ∗ in red (Characteristic hydrogen of Dppf) ※ in purple (Characteristic hydrogen of the methylene group of N-2-Propyn-1-ylcyclohexanamine) ⁑ in orange (The methyl hydrogen peak (1.11 ppm) of the C≡C^{t}Bu ligand disappears.) **c** ^{31}P NMR spectra of Ag_4* NC R^1 = cyclohexyl, Ag_4 NC, and Dppf.

1a and that the C≡C bond of **1a** was activated by Ag_4 NC, which was related to the dehydrogenation activation of **1a**[49]. To obtain direct evidence of the interaction between Ag_4 NC and **1a**, we captured the Ag_4* NC intermediate by ESI-MS. As shown in Fig. 2a, the mass spectrum peaks of Ag_4* NC (R^1 = benzyl) were detected and calculated to be 661.0 m/z and 914.0 m/z (Simulation: 661.3 m/z = [Ag+Dppf]$^+$, 914.3 m/z = [1/2Ag_4-C≡C^{t}Bu + C≡CCH$_2$NHBn-CH$_3$OH]$^+$ respectively). The ESI-MS peaks of Ag_4* NC (R^1 = benzyl) corresponded exactly to those of Ag_4 NC (661.3 m/z and 851.3 m/z, Simulation: 661.3 m/z = [Ag+Dppf]$^+$, 851.3 m/z = [1/2Ag_4-CH$_3$OH]$^+$, respectively). Notably, Ag_4* (R^1 = benzyl) species were also successfully detected by ESI-MS in the reaction solution (Ag_4 + **1a** + CO_2), suggesting that Ag_4* NC is a key intermediate in the catalytic cycle (Supplementary Fig. 6a). To confirm this hypothesis, we isolated and verified the activity of Ag_4* NC (R^1 = benzyl). The experimental results showed that the activity of Ag_4* NC and Ag_4 NC was similar, confirming that Ag_4* NC was the key intermediate. The isolated Ag_4* NC (R^1=cyclohexyl), Ag_4 NC, dppf ligand and substrate **4a** were characterized by ^{1}H NMR (Fig. 2b). The ^{1}H NMR spectrum of Ag_4 NC contains the characteristic peak attributed to the hydrogen of the dppf and tert-butylvinyl ligands, and the ratio of the intensities of the peaks attributed to the benzene ring hydrogen (7.49 ppm) on the dppf ligand to the metal ring hydrogen (4.49 ppm, 4.03 ppm) and the C≡C^{t}Bu ligand methyl hydrogen (1.11 ppm) was 40:8:8:18, and some peak shifts were observed. This was consistent with the molecular formula of Ag_4 NC, which reflects the structural integrity and high matching of the Ag_4 NC. Compared with the ^{1}H NMR spectrum of **4a**, the ^{1}H NMR spectrum of Ag_4* NC showed shifts in the characteristic peak of the hydrogen of the cyclohexyl group (marked by the black dashed circle) and the methylene hydrogen peak (purple symbol) in the substrate HC≡CCH$_2$NHCy (**4a**), while the methyl hydrogen peak of the C≡C^{t}Bu ligand (1.11 ppm) disappeared. Additionally, the ratio of the intensities of the peaks attributed to the methylene hydrogen of C≡CCH$_2$NHCy (3.69 ppm), the monocyclic hydrogen of the dppf ligand (4.10 ppm, 4.34 ppm) and the benzene ring hydrogen (7.40 ppm) was 3.8:8:8:40.5, indicating that the structure of the Ag_4* NC molecule was similar to that of the Ag_4 NC molecule, including two dppf ligands and two C≡CCH$_2$NHCy ligands. At the same time, it can be seen from the ^{31}P spectrum (Fig. 2c) that the structure of Ag_4* NC is similar to that of

Ag_4 NC, and there is no free P ligand in the system. Moreover, the other substrates [HC≡CCH$_2$NHCy (**4a**, R^1 = cyclohexyl) and HC≡CCH$_2$NH^{n}Bu (**3a**, R^1 = normal-butyl)] were selected for the primitive reaction with Ag_4 NC. The ESI-MS results showed two ionic peaks located at 661.0 m/z and 906.0 m/z (Simulation: 661.3 m/z = [Ag+Dppf]$^+$, 906.3 m/z = [1/2Ag_4-C≡C^{t}Bu+C ≡ CCH$_2$NHCy-CH$_3$OH]$^+$, respectively), along with peaks at 661.0 m/z and 880.0 m/z (Simulation: 661.3 m/z = [Ag+Dppf]$^+$, 880.3 m/z = [1/2Ag_4-C≡C^{t}Bu + C≡CCH$_2$NH^{n}Bu-CH$_3$OH]$^+$, respectively). Meanwhile, the Ag_4* (R^1 = cyclohexyl) species was also successfully identified in the reaction solution (Ag_4 + **4a** + CO_2) (Fig. 2a and Supplementary Fig. 6b).

Consistent with the experimental observations, the ligand exchange of 3,3-dimethyl-1-butyne (BH) with N-benzylprop-2-yn-1-amine (AH) was found to be thermodynamically feasible (exergonic by 6.4 kcal/mol, Fig. 3b). After that, two main types of mechanisms, depending on whether carboxylation occurs on the incoming A substrate (via ligand exchange, Path I) or an extra AH substrate (Path II, Supplementary Fig. 15 and Fig. 3b), were investigated. In path I, the coordinated A group on $Ag_4P_4A_2$ first reacted with DBU, and this step was slightly endergonic by 7.7 kcal/mol (Fig. 3b). Thereafter, carboxylation with CO_2 occurred on $Ag_4P_4A_2$-2 to generate the intermediate $Ag_4P_4A_2c$-1 (c represents CO_2), with a low activation barrier of 12.1 kcal/mol owing to the high nucleophilicity of the deprotonated amino group. Subsequent cyclization then occurred with a barrier of 16.3 kcal/mol. The resulting intermediate $Ag_4P_4A_2c$-2 then underwent protonation and ligand exchange to complete the catalytic cycle. Overall, the Ag_4-catalyzed cycloaddition of N-benzylprop-2-yn-1-amine was highly exergonic by -37.7 kcal/mol, and the carboxylation step was the rate-determining step ($Ag_4P_4A_2$-2 → $Ag_4P_4A_2c$-1). Path II started with the coordination of an extra AH substrate, preferentially via an amino group, to form $Ag_4P_4A_3H$-1 (Supplementary Figs. 15, 16 and Fig. 3b). Similar to the overall transformation in Path I, deprotonation, carboxylation, cyclization, and protonation then occurred to generate the final product. However, the overall energy demands for Path II were 4.4 kcal/mol higher than those for Path I (26.0 vs. 21.6 kcal/mol in Fig. 3b and Supplementary Fig. 15). Of note, in this study, some other pathways, including deprotonation and carboxylation on $Ag_4P_4A_3H$-1, were also examined but were excluded because of their relatively high energy demands (Supplementary Fig. 17). In this context, Path I was the most feasible pathway. Moreover, the carboxylation process of path I was experimentally investigated by ^{13}C NMR and ESI-MS. As shown in Supplementary Fig. 19, the ^{13}C NMR carbon spectrum shows that the characteristic peaks of raw material **1a** gradually weakened with the insertion of carbon dioxide. Meanwhile, new peaks assigned to the products gradually emerge and enhance. The characteristic peak signal changed significantly within 0.5 h, so we monitor the ESI-MS spectrum of the reaction solution during this period. To be noted, intermediate species IV (Fig. 3) was successfully detected by ESI-MS when Ag_4 NC, **1a** and CO_2 were mixed for 15 min. The mass peak of [Ag_4C≡CCH$_2$NHBnC=CCH$_2$CH$_2$O$_2$NBn (Dppf)$_2$]$^+$ was detected at 1871.6 m/z (simulation: 1871.6 m/z) (Supplementary Fig. 20), coincident with the species IV on path I of DFT calculations (Fig. 3b, via

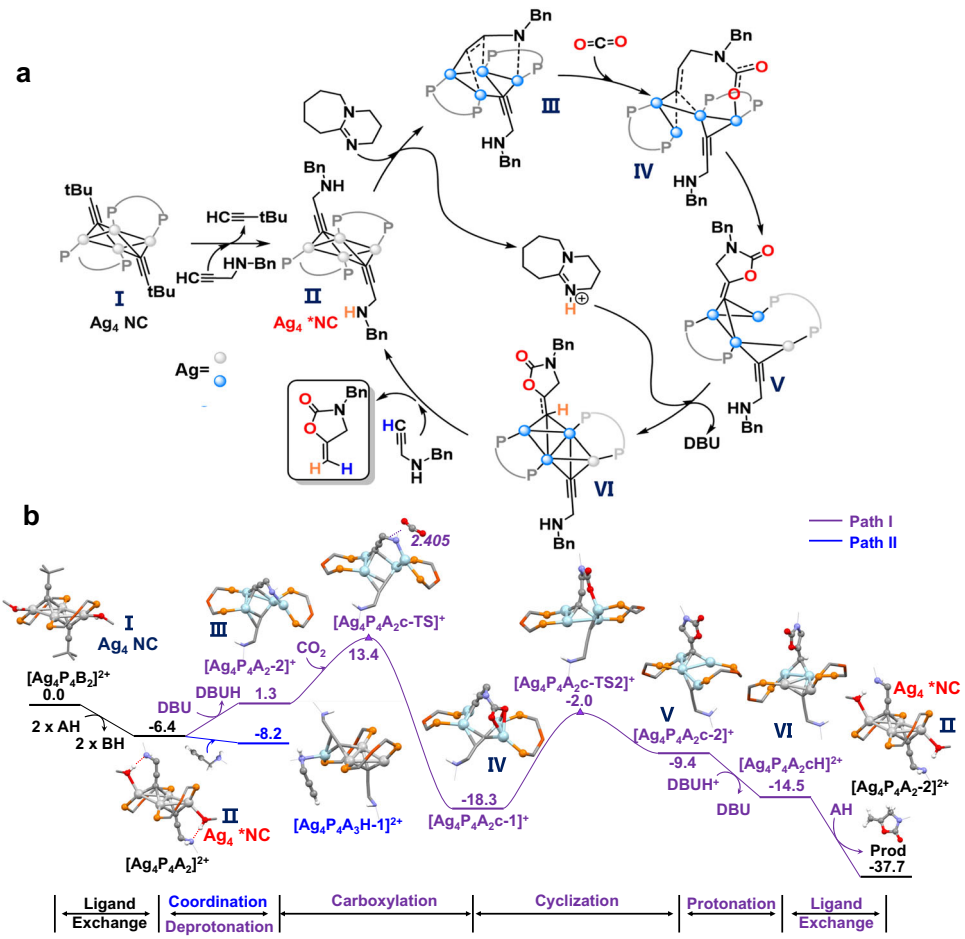

Fig. 3 | Proposed mechanism and calculation of the relative Gibbs free energies for Ag_4 NC. a Proposed mechanism by Ag_4 NC. **b** The relative Gibbs free energies, in bold. Gibbs free energy profiles of the Ag_4 NC on carboxylation of N-benzylprop-2-yn-1-amine. Abbreviated labels: AH (N-benzylprop-2-yn-1-amine,**1a**); BH (3,3-Dimethyl-1-butyne); c(CO_2); P_2(dppf). For clarity, the two MeOH molecules, all H atoms (unless the reaction site), and the benzyl group on N-benzylprop-2-yn-1-amine were omitted in all structures except for $Ag_4P_4B_2$ and $Ag_4P_4A_2$. Silver: silver and light blue.

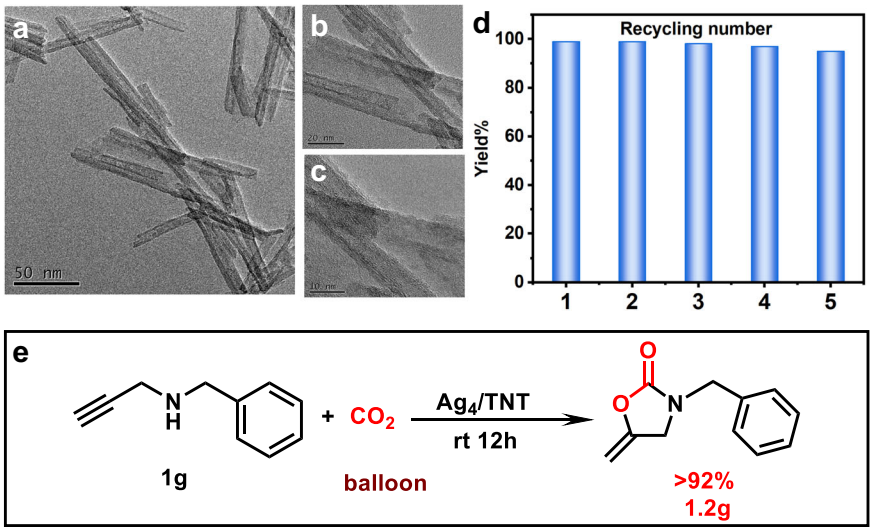

Fig. 4 | Characterization and applications of Ag_4/TNT. a–c TEM images of Ag_4/TNT. **d** Recoverability of Ag_4/TNT catalysts in the cyclization of propargylamine with CO_2. reaction conditions: Ag_4/TNT (50 mg, 1.6 wt% loading of NCs), N-benzylprop-2-yn-1-amine (0.5 mmol), DBU (0.05 mmol), acetonitrile (1.0 mL), 25 °C, 12 h, CO_2 balloon. **e** Gram scale experiment.

ligand exchange). The tetranuclear Ag_4 core was pivotal in stabilizing the deprotonated amino group in $Ag_4P_4A_2$-2 and the anionic carboxylic group in $Ag_4P_4A_2$c-1. Such an interaction was unlikely in the Ag_2 system, as Ag-N coordination resulted in remarkable structural distortion in the diphosphine ligand. This was also the reason the yield of the Ag_2 system was significantly lower than that of the Ag_4 system (Supplementary Fig. 18). Based on the above, we proposed a mechanism for the cyclization of propargylamine with CO_2 catalyzed by Ag_4 NC (Fig. 3a). Obviously, Ag_4 NC first interacted with the propylamine substrate to produce the dehydrogenation activation product Ag_4* NC, which remained in the form of Ag_4* NC after cyclization. Throughout the catalytic process, activation of the substrate required coordination between multiple Ag atoms (the blue atoms represent the active Ag atoms), confirming the reaction pathways that are inaccessible to the Ag single-atom catalyst and Ag_2 NC.

To understand its applicability, the Ag_4/TNT nanocomposite was successfully synthesized, which characterized by solid-state UV, XRD, TEM, XPS and element mapping (see Fig. 4 and Supplementary Figs. 7–11 for details). The Ag_4/TNT nanocomposites demonstrated the same activity as Ag_4 NC, while TNT carrier was inactive (Supplementary Fig. 12). In this scenario, a recycling experiment was performed with **1a** as the substrate, and the reaction efficiency did not show significant changes even after five runs (Fig. 4d and Supplementary Fig. 13). To determine the practicability of this transformation, a scale-up experiment afforded 3-benzyl-5-methylene-2-oxazolone in 1.2 g and >92% yield, which is comparable to previous results (Fig. 4e).

In summary, alkyne-protected low-nuclear Ag_4 nanocluster (NC) is designed to catalyze the cyclization of propargylamine with CO_2. As expected, the low-nuclear Ag_4 NC achieves the highest TON value of 5746.2, significantly higher than that of reported catalysts and the corresponding Ag_2 NC, Ag_6 NC and Ag_9 NC. In addition, the Ag_4 NC successfully achieves the cyclization of propargylamine with CO_2 under mild conditions. In the elementary reaction of Ag_4 NC with substrates, including $HC{\equiv}CCH_2NHBn$, $HC{\equiv}CCH_2NHCy$ and $HC{\equiv}CCH_2NH^nBu$, we capture three Ag_4* NC intermediates and confirm their structures by Electrospray ionization (ESI). Density functional theory (DFT) calculations further confirm the key role of four Ag atoms, revealing the feasibility and importance of low-nuclear catalysts at the atomic level. Importantly, the Ag_4/TNT (functional titanate nanotubes) nanocomposite afford the product at the gram scale. Therefore, the customized Ag_4 catalyst improves the reaction activity while exerting the atomic economy similar to that of single atom catalyst, which has advantages in reducing cost. The present work provides a new perspective on the mechanism of the cyclization of propargylamine with CO_2, which provides further support for the design of further atomic level catalysts and their efficient utilization.

Methods

Characterizations

The UV−vis. spectra were recorded on a Techcomp UV 1000 spectrophotometer. Transmission electron microscopy (TEM) was conducted on a JEM-2100 microscope with an accelerating voltage of 200 kV. The FT-IR spectra were recorded with a Bruker Tensor 27 instrument. The X-ray diffraction (XRD) patterns were obtained on Smart Lab 9 KW with Cu Kα radiation. The NCs loaded on the TNT catalyst support were determined by Inductively Coupled Plasma Mass Spectrometry (ICP-MS). The X-ray photoelectron spectroscopy (XPS) measurements were conducted on ESCALAB 250Xi. Electrospray ionization mass spectra (ESI-MS) were recorded using a Waters UPLC H-class/Xevo G2-XS Qtof mass spectromete.

Catalytic activity

A typical "the cyclization of propargylamine with CO_2" reaction was used to evaluate the catalytic performance of Ag_4 NC. Ag_4 NC (0.4 mg, 0.2×10^{-3} mmol), propargylamines (0.5 mmol), and 1,8-Diazabicyclo [5.4.0] undec-7-ene(DBU) (0.05 mmol) were added to acetonitrile (1 mL) in the reaction tube. The reaction stirring for 2 h at 25 °C with the balloon in Carbon dioxide atmosphere. After the reaction stopped, The reaction solution was diluted by dichloromethane, The conversion and selectivity were determined by GC analysis and column chromatography (EtOAc/PE = 1:5).

Data availability

Data supporting the findings of this work are available within the article and its Supplementary Information. The data that support the findings of this study are available from the corresponding author upon request. The X-ray crystallographic structures reported in this work have been deposited at the Cambridge Crystallographic Data Center (CCDC) under deposition numbers 2254886 for [Ag_2dppf$_3$]. These data can be obtained free of charge from the CCDC via https://www.ccdc.cam.ac.uk/structures/.

References

1. Yang, Y. et al. Operando studies reveal active Cu nanograins for CO_2 electroreduction. *Nature* **614**, 262–269 (2023).
2. Jiao, J. et al. Copper atom-pair catalyst anchored on alloy nanowires for selective and efficient electrochemical reduction of CO_2. *Nat. Chem.* **11**, 222–228 (2019).
3. Woldu, A. R., Huang, Z., Zhao, P., Hu, L. & Astruc, D. Electrochemical CO_2 reduction (CO_2RR) to multi-carbon products over copper-based catalysts. *Coord. Chem. Rev.* **454**, 214340 (2022).
4. Cheng, D. et al. Catalytic synthesis of formamides by integrating CO_2 capture and morpholine formylation on supported iridium catalyst. *Angew. Chem., Int. Ed.* **61**, e202202654 (2022).
5. Zhou, Y. et al. Long-chain hydrocarbons by CO_2 electroreduction using polarized nickel catalysts. *Nat. Catal.* **5**, 545–554 (2022).
6. Jiao, X. et al. Fundamentals and challenges of ultrathin 2D photocatalysts in boosting CO_2 photoreduction. *Chem. Soc. Rev.* **49**, 6592–6604 (2020).
7. Ding, M., Flaig, R. W., Jiang, H.-L. & Yaghi, O. M. Carbon capture and conversion using metal–organic frameworks and MOF-based materials. *Chem. Soc. Rev.* **48**, 2783–2828 (2019).
8. Cai, T. et al. Cell-free chemoenzymatic starch synthesis from carbon dioxide. *Science* **373**, 1523–1527 (2021).
9. Yun, Y. et al. Design and remarkable efficiency of the Robust Sandwich cluster composite nanocatalysts ZIF-8@Au_{25}@ZIF-67. *J. Am. Chem. Soc.* **142**, 4126–4130 (2020).
10. Liu, Y. et al. Central doping of a foreign atom into the silver cluster for catalytic conversion of CO_2 toward C-C bond formation. *Angew. Chem. Int. Ed.* **57**, 9775–9779 (2018).
11. Fang, X. et al. Poly(ionic liquid)s for Photo-Driven CO_2 Cycloaddition: Electron Donor-Acceptor Segments Matter. *Adv. Sci.* **10**, 2206687 (2023).
12. Li, G. et al. Precisely Constructed Silver Active Sites in Gold Nanoclusters for Chemical Fixation of CO_2. *Angew. Chem. Int. Ed.* **60**, 10573–10576 (2021).
13. Zhao, M. et al. Ambient Chemical Fixation of CO_2 Using a Robust Ag_{27} Cluster-based Two-dimensional Metal-organic Framework. *Angew. Chem. Int. Ed.* **59**, 20031–20036 (2020).
14. Kim, A. N. et al. Iridium-catalyzed enantioselective and diastereoselective hydrogenation of 1,3-disubstituted isoquinolines. *ACS Catal.* **10**, 3241–3248 (2020).
15. Siddiqui, A. M. et al. Design, synthesis, and biological evaluation of spiropyrimidinetriones oxazolidinone derivatives as antibacterial agents. *Bioorg. Med. Chem. Lett.* **28**, 1198–1206 (2018).
16. Gu, A.-L. et al. Highly efficient conversion of propargylic alcohols and propargylic amines with CO_2 activated by noble-metal-free catalyst Cu_2O@ZIF-8. *Angew. Chem. Int. Ed.* **61**, e202114817 (2022).
17. Cui, H.-Y., Zhang, Y.-X., Cao, C.-S., Hu, T.-D. & Wu, Z.-L. Engineering noble-metal-free metal–organic framework composite catalyst for efficient CO_2 conversion under ambient conditions. *Chem. Eng. J.* **451**, 138764 (2023).
18. Cao, C.-S. et al. Highly efficient conversion of propargylic amines and CO_2 catalyzed by noble-metal-free [Zn_{116}] nanocages. *Angew. Chem. Int. Ed.* **59**, 8586–8593 (2020).
19. Zhang, Y. et al. Controllable encapsulation of silver nanoparticles by porous pyridine-based covalent organic frameworks for efficient CO_2 conversion using propargylic amines. *Green Chem.* **24**, 930–940 (2022).
20. Liu, P. et al. Synergy between palladium single atoms and nanoparticles via hydrogen spillover for enhancing CO_2 photoreduction to CH_4. *Adv. Mater.* **34**, 2200057 (2022).
21. Yang, H. B. et al. Atomically dispersed Ni(i) as the active site for electrochemical CO_2 reduction. *Nat. Energy.* **3**, 140–147 (2018).
22. Du, P. et al. Single-atom-driven dynamic carburization over Pd_1–FeO_x catalyst boosting CO_2 conversion. *Chem.* **8**, 3252–3262 (2022).
23. Ou, H. et al. Atomically dispersed Au-assisted C–C coupling on red phosphorus for CO_2 photoreduction to C_2H_6. *J. Am. Chem. Soc.* **144**, 22075–22082 (2022).
24. Sun, Z. et al. Understanding Synergistic Catalysis on Cu-Se Dual Atom Sites via Operando X-ray Absorption Spectroscopy in Oxygen Reduction Reaction. *Angew. Chem. Int. Ed.* **62**, e202217719 (2023).
25. Yi, J.-d, Gao, X., Zhou, H., Chen, W. & Wu, Y. Design of Co-Cu diatomic site catalysts for high-efficiency synergistic CO_2 electroreduction at industrial-level current density. *Angew. Chem. Int. Ed.* **61**, e202212329 (2022).
26. Yao, D. et al. Inter-Metal Interaction with a Threshold Effect in NiCu Dual-Atom Catalysts for CO_2 Electroreduction. *Adv. Mater.* **35**, 2209386 (2023).
27. Swain, S., Altaee, A., Saxena, M. & Samal, A. K. A comprehensive study on heterogeneous single atom catalysis: Current progress, and challenges. *Coord. Chem. Rev.* **470**, 214710 (2022).
28. Zhang, N. et al. A supported Pd_2 dual-atom site catalyst for efficient electrochemical CO_2 reduction. *Angew. Chem. Int. Ed.* **60**, 13388–13393 (2021).
29. Ding, T. et al. Atomically precise dinuclear site active toward electrocatalytic CO_2 reduction. *J. Am. Chem. Soc.* **143**, 11317–11324 (2021).
30. Ren, Y., Yang, Y., Zhao, Y.-X. & He, S.-G. Conversion of methane with oxygen to produce hydrogen catalyzed by triatomic Rh_3^- cluster anion. *JACS Au* **2**, 197–203 (2022).
31. Sun, Y. et al. Supported Cu_3 clusters on graphitic carbon nitride as an efficient catalyst for CO electroreduction to propene. *J. Mater. Chem. A* **10**, 14460–14469 (2022).
32. Wang, L. et al. Cooperative sites in fully exposed Pd clusters for low-temperature direct dehydrogenation reaction. *ACS Catal.* **11**, 11469–11477 (2021).
33. Wang, X. et al. Atomic-precision Pt_6 nanoclusters for enhanced hydrogen electro-oxidation. *Nat. Commun.* **13**, 1596 (2022).
34. Song, Y. et al. Highly reversible solid-state lithium-oxygen batteries by size-matching between Fe-Fe cluster and Li_2-xO_2. *Adv. Energy Mater.* **13**, 2203660 (2023).
35. Ling, C. et al. Atomic-layered Cu_5 Nanoclusters on FeS_2 with dual catalytic sites for efficient and selective H_2O_2 activation. *Angew. Chem. Int. Ed.* **61**, e202200670 (2022).
36. Fang, Y. et al. Insight into the mechanism of the CuAAC reaction by capturing the crucial Au_4Cu_4–π-Alkyne intermediate. *J. Am. Chem. Soc.* **143**, 1768–1772 (2021).
37. Deng, Y. et al. Embedding ultrasmall Au clusters into the pores of a covalent organic framework for enhanced photostability and photocatalytic performance. *Angew. Chem. Int. Ed.* **59**, 6082–6089 (2020).
38. Jiang, Y. et al. N-heterocyclic carbene-stabilized ultrasmall gold nanoclusters in a metal-organic framework for photocatalytic CO_2 reduction. *Angew. Chem. Int. Ed.* **60**, 17388–17393 (2021).
39. Cook, A. W., Jones, Z. R., Wu, G., Scott, S. L. & Hayton, T. W. An organometallic Cu_{20} nanocluster: synthesis, characterization, immobilization on Silica, and "Click" chemistry. *J. Am. Chem. Soc.* **140**, 394–400 (2018).
40. Wan, X.-K., Wang, J.-Q., Nan, Z.-A. & Wang, Q.-M. Ligand effects in catalysis by atomically precise gold nanoclusters. *Sci. Adv.* **3**, e1701823 (2017).
41. Wang, Y. et al. Atomically precise alkynyl-protected metal nanoclusters as a model catalyst: observation of promoting effect of surface ligands on catalysis by metal nanoparticles. *J. Am. Chem. Soc.* **138**, 3278–3281 (2016).

42. Lei, Z., Wan, X.-K., Yuan, S.-F., Guan, Z.-J. & Wang, Q.-M. Alkynyl approach toward the protection of metal nanoclusters. *Acc. Chem. Res.* **51**, 2465–2474 (2018).
43. Hu, J.-W. et al. Alkynyl-anchored silver nanoclusters in lanthanide metal-organic framework for luminescent thermometer and CO_2 cycloaddition. *Nano Res.* **16**, 7452–7458 (2023).
44. Yan, J., Teo, B. K. & Zheng, N. Surface chemistry of atomically precise coinage–metal nanoclusters: from structural control to surface reactivity and catalysis. *Acc. Chem. Res.* **51**, 3084–3093 (2018).
45. Cook, A. W., Nguyen, T.-A. D., Buratto, W. R., Wu, G. & Hayton, T. W. Synthesis, characterization, and reactivity of the group 11 hydrido clusters $[Ag_6H_4(dppm)_4(OAc)_2]$ and $[Cu_3H(dppm)_3(OAc)_2]$. *Inorg. Chem.* **55**, 12435–12440 (2016).
46. Alamer, B. J. et al. $[Ag_9(1,2\text{-}BDT)_6]^{3-}$: how square-pyramidal building blocks self-assemble into the smallest silver nanocluster. *Inorg. Chem.* **60**, 4306–4312 (2021).
47. Liu, K.-G. et al. Ultrasonic-assisted fabrication of thin-film electrochemical detector of H_2O_2 based on ferrocene-functionalized silver cluster. *Ultrason. Sonochem.* **56**, 305–312 (2019).
48. Ghosh, S. et al. Utility of Silver nanoparticles embedded covalent organic frameworks as recyclable catalysts for the sustainable synthesis of cyclic carbamates and 2-Oxazolidinones via atmospheric cyclizative CO_2 capture. *ACS Sustain. Chem. Eng.* **8**, 5495–5513 (2020).
49. Liu, Y. et al. Central doping of a foreign atom into the silver cluster for catalytic conversion of CO_2 toward C–C bond formation. *Angew. Chem. Int. Ed.* **57**, 9775–9779 (2018).

Acknowledgements

We acknowledge financial support by the National Natural Science Foundation of China under grant number 21972001 (H.T.S.) and 21871001 (M.Z.Z.) and Natural Science Foundation of Anhui Province, Anhui University under grant number 2008085MB37(H.T.S.).

Author contributions

L.L. performed experiments and paper writing. Y.L. performed DFT theoretical studies and paper writing. Y.L.D., H.F.L., Y.P.Y., Z.Y.Z. participated in the data analysis and revision; H.T.S., H.Z.Y., and M.Z.Z. contributed to the design of the study, data analysis, and paper writing.

Competing interests

The authors declare no competing interests.

Additional information

Supplementary information The online version contains supplementary material available at https://doi.org/10.1038/s41467-023-42723-3.

Correspondence and requests for materials should be addressed to Hongting Sheng, Haizhu Yu or Manzhou Zhu.

Peer review information *Nature Communications* thanks the anonymous reviewers for their contribution to the peer review of this work. A peer review file is available.